Ab initio calculation of electron-capture cross sections in $H^+ + BeH$ collisions

I. Rabadán,[1] L. Méndez,[1] J. W. Gao,[2,3] Y. Wu,[2] and J. G. Wang[2]

[1]*Laboratorio Asociado al CIEMAT de Física Atómica y Molecular en Plasmas de Fusión, Departamento de Química, módulo 13, Universidad Autónoma de Madrid, Cantoblanco, E-28049 Madrid, Spain*

[2]*Institute of Applied Physics and Computational Mathematics, 100088 Beijing, China*

[3]*Sorbonne Universités, UPMC Université Paris 06, Laboratoire de Chimie Physique Matière et Rayonnement, 75005 Paris, France*

(Received 29 May 2017; revised manuscript received 31 July 2017; published 19 September 2017)

We present calculations of electron-capture cross sections in collisions of H^+ with BeH molecules in the energy range 25 eV $< E <$ 10 keV. We discuss the validity of the models employed to describe nonadiabatic ion-molecule collisions, specifically the eikonal approximation, the Franck-Condon approximation, and the isotropic approximation to obtain orientation-averaged cross sections, which is based on the infinite-order sudden approximation. The calculation using the Franck-Condon approximation leads to a total electron-capture cross section that is practically independent of the collision energy with a value of around 25 $Å^2$. The calculations using the more accurate sudden vibrational approximation indicate that the Franck-Condon approximation overestimates the electron-capture cross section by at most 20%. At $E < 1$ keV, the main product of the electron-capture process is the formation of $BeH^+(2\,^1\Sigma^+)$+H(1s). At higher energies, the cross sections for formation of $BeH^+(2\,^1\Sigma^+)$+H(1s) and $BeH^+(1\,^3\Sigma^+)$+H(1s) are practically identical. The Coriolis couplings are particularly relevant to the mechanism of this reaction, which precludes the merging of semiclassical (including Coriolis couplings) and quantal results (neglecting Coriolis couplings) in the energy range of the present calculation.

DOI: 10.1103/PhysRevA.96.032714

I. INTRODUCTION

A key issue in the design of future fusion tokamaks is the choice of plasma-facing materials. In this respect, carbon-containing components, previously used in tokamaks, present high erosion and cause high tritium retention. These important drawbacks have motivated that carbon will not be used in the first wall of ITER [1], which will contain beryllium in the main chamber and tungsten in the divertor. In particular, beryllium has been selected as the plasma-facing component of the ITER main chamber because it leads to relatively low impurity concentration and low fuel retention. An ITER-like-wall (ILW) is currently installed in the Joint European Torus (JET) [2] and several experiments have already been carried out in order to understand the erosion of the first wall and the material migration (see Ref. [3] and references therein).

The erosion of Be surfaces by D plasmas have been studied in PISCES-B experiments and molecular dynamics simulations [4,5], which showed that the erosion of the Be wall takes place by physical sputtering, and there is also a chemical-assisted physical sputtering mechanism that leads to the release of molecular species, in particular BeD. The importance of this mechanism has been pointed out in JET-ILW experiments [6,7]. The BeD molecules formed in the plasma-wall interaction are ionized and dissociated by collision with the main plasma components, and the rate coefficients for these processes are required in transport modeling codes, such as the Monte Carlo code ERO [8]. However, while the rate coefficients for electron collisions are currently incorporated in the simulations, the heavy-particle collisions are not considered. In particular, we are interested in the electron-capture (EC) reaction

$$H^+ + BeH(X\,^2\Sigma^+) \rightarrow H + BeH^+ \qquad (1)$$

that takes place in the collision of BeH with protons (deuterons). Given that the cross sections for this reaction have not been measured yet in beam experiments, their values are only accessible theoretically, and no previous calculations have been carried out hitherto because of the difficulties associated to the treatment of the vibrorotational molecular degrees of freedom.

Several well-established theoretical methods are currently employed for describing EC in ion-atom collisions (see, e.g., Ref. [9]). For instance, at low impact energies it is appropriate to apply a quantal formalism with a molecular basis. As the energy increases, semiclassical treatments with molecular or atomic bases are used and, at high energies, classical trajectory Monte Carlo (CTMC) and continuum-distorted-wave treatments. In the past ten years, the computational power has made it possible to solve numerically the time-dependent Schrödinger equation. The range of applicability of these methods is known; they have been applied to systems with one active electron to provide accurate total cross sections, compared to the available experimental values. For instance, in the benchmark system He^{2+}+ H(1s), Minami *et al.* [10] reported total and n-partial cross sections in overall good agreement with the experiments. By comparing different methods, they reported an estimated uncertainty smaller 10% in the energy range $1 < E < 1000$ keV, and uncertainties between 1% and 30% for the n-partial cross sections, with the largest uncertainties associated to the smallest cross sections. Recently, Jorge *et al.* [11] estimated uncertainties of about 15% in n-partial cross sections in Be^{4+}+ H(1s) collisions. Obviously, it is difficult to obtain similar accuracies for many-electron systems. At high energy, the independent electron approximation is in general applied, which limits the accuracy of the theoretical predictions. At low energies, the calculations for many-electron systems employ molecular wave functions, obtained by means of quantum chemistry calculations. An example of the merging of different methods can be found in Ref. [12], but there is not an estimate of the uncertainties associated to the calculated values.

The theoretical description of ion-molecule collisions does not simply involve an extension of the ion-atom techniques to more complex systems. The main difference is the presence of the vibrorotational degrees of freedom. However, at not-too-low collision energies ($E \gtrsim 0.25$ keV/u), the vibrational motion is slow compared to the ion-molecule relative motion, and one can assume that the molecule internal coordinates are fixed during the collision, which is the basis of the sudden approximation for rotation and vibration (see Ref. [13]). Within this approximation, the solution of the ion-molecule problem reduces to a set of calculations for each nuclear configuration, and each of them is similar to an ion-atom collision calculation, which permits one to modify the ion-atom codes and to apply them to study ion-molecule collisions. However, even within the sudden approximation, there are two additional characteristics of ion-molecule collisions. First, the experiments are usually carried out with gas-phase targets where the molecules are randomly oriented and, accordingly, the calculation must yield orientation-averaged cross sections. Second, in systems with three nuclei or more, the electronic potential energies display conical intersections, which yield singular dynamical couplings between the corresponding adiabatic molecular wave functions. Since the description of the collision system at low energies is generally performed in a molecular basis, it is necessary to construct an alternative (diabatic) set without singularities; this is the so-called regularization process.

In this work we have calculated the cross sections for reaction (1) in the energy range 25 eV $< E <$ 10 keV, employing a basis set of electronic functions of the BeH_2^+ molecule. Our treatment is based on the application of the sudden approximation for molecular vibration and rotation. The use of sudden approximations for molecular rotation, within a quantum-mechanical framework, has been discussed in detail in several reviews (e.g., Refs. [14,15]) and the so-called infinite order sudden (IOS) approximation has been applied to calculate EC cross sections [16–18]. At collision energies above 200 keV/u, the quantum-mechanical treatment of inelastic ion-molecule collisions becomes cumbersome and a semiclassical approximation is appropriate. In this respect, the pioneering work of Schinke [19] applied the sudden approximation for rotation in the semiclassical treatment of vibrational excitation in $H^+ + H_2$ collisions. The application of the sudden approximation for vibration and rotation in the semiclassical framework was implemented in Ref. [20]. Most of the previous works on ion-diatomic collisions have been carried out for the benchmark system $H^+ + H_2$. Besides the works already mentioned [16–19], the EC reaction has been studied in the works of Refs. [21–23], at impact energies of a few keV/u, and in the CTMC calculations of Refs. [24,25] at higher energies (10 keV $\lesssim E \lesssim$ 1 MeV). The calculations at high energy (1 MeV) [26] predicted an interference effect, observed in measurements [27] of EC cross section as a function of the molecular orientation. All these calculations assumed that the molecule remains at the equilibrium distance during the collision. Ionization of H_2 in proton collisions has been extensively studied at $E =$ 75 keV. Namely, cold-target-ion-momentum-spectroscopy experiments and continuum-distorted-wave eikonal-initial-state calculations [28,29] showed the presence of interference structures in the double-differential cross sections as functions of the projectile scattering angle, and, more recently, triple-differential cross sections have been considered [30–32].

The validity of the sudden approximation for rotation and vibration has been discussed for the benchmark system $H^+ + H_2$ in Ref. [33], where it was shown that it is not appropriate at low collision energies ($E \lesssim 200$ eV), because the transitions leading to the EC process take place between quasidegenerate vibronic levels, as suggested in Ref. [34], and a method beyond the sudden approximation must be applied as in the calculations of Ref. [35]. In order to compare with beam experiments with gas-phase targets, the cross section must be averaged with respect to the molecule orientation (see Ref. [20]). Similar averaging procedures were applied in Ref. [36] and extended to collisions with three-center molecules in Refs. [37,38].

In order to gauge the accuracy of the calculation, we have combined several computational techniques. In particular, at relatively low energies, the accuracy of the cross sections is determined by that of the molecular calculation, and we have compared the potential energy surfaces and dynamical couplings obtained with two quantum chemistry packages. First is the package MELDF (see, e.g., Ref. [39]), which allows us to calculate potential energy surfaces (PESs) and wave functions with a multireference configuration-interaction method. This code was modified to calculate numerically the dynamical couplings in Ref. [40]. A numerical differentiation technique was also incorporated into the MRDCI code [41], and the results of applying both packages are compared.

The paper is organized as follows: In Sec. II, we summarize the theoretical models employed. In Sec. III, we present the molecular calculations for the BeH_2^+ ion and show the energies and nonadiabatic couplings required to perform the dynamical calculation. The EC cross sections are displayed in Sec. IV, and a brief summary is presented in Sec. V. Atomic units are used unless otherwise stated.

II. THEORETICAL METHOD

A. Quantum-mechanical treatment

In the quantum-mechanical formalism, the collision wave function is a solution of the stationary Schrödinger equation,

$$H(\boldsymbol{r},\boldsymbol{R},\boldsymbol{\rho})\Psi(\boldsymbol{r},\boldsymbol{R},\boldsymbol{\rho}) = E\Psi(\boldsymbol{r},\boldsymbol{R},\boldsymbol{\rho}), \tag{2}$$

with $H = T_R + H_{\rm int}$, and the internal Hamiltonian has the form

$$H_{\rm int}(\boldsymbol{r},\boldsymbol{R},\boldsymbol{\rho}) = T_\rho + H_{\rm el}(\boldsymbol{r},\boldsymbol{R},\boldsymbol{\rho}), \tag{3}$$

where $\boldsymbol{R}$ and $\boldsymbol{\rho}$ are the Jacobi coordinates of a three-nuclei system (Fig. 1), and $\boldsymbol{r}$ is the set of electronic coordinates. T_R and T_ρ are the kinetic energy operators associated to $\boldsymbol{R}$ and $\boldsymbol{\rho}$, respectively. $H_{\rm el}$ is the clamped-nuclei Born-Oppenheimer electronic Hamiltonian of the three-center system:

$$H_{\rm el}(\boldsymbol{r},\boldsymbol{R},\boldsymbol{\rho}) = T_r + V(\boldsymbol{r},\boldsymbol{R},\boldsymbol{\rho}). \tag{4}$$

In order to introduce the sudden approximation, it is useful to define the internal Hamiltonian for the nuclear motion of the molecular target:

$$H_{\rm BeH} = T_\rho + V_{\rm BeH}(\rho) \tag{5}$$

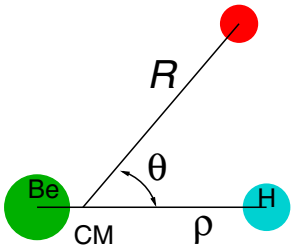

FIG. 1. Internal coordinates (R,ρ,θ) for the $p+$BeH system. CM is the position of the BeH center of mass.

and we assume that the initial vibrorotational state of the molecule is $\rho^{-1}Y_{jm}(\hat{\boldsymbol{\rho}})\chi_0(\rho)$, with energy ε_{0j}. At not-too-low collision energies, the vibrorotational motion is slow compared to the projectile motion and we introduce a sudden approximation for rotation and vibration, where the approximate solution of Eq. (2) is written in the form

$$\Psi_0^{jm} = \rho^{-1}Y_{jm}(\hat{\boldsymbol{\rho}})\chi_0(\rho)\psi(\boldsymbol{r},\boldsymbol{R};\boldsymbol{\rho}). \tag{6}$$

The function $\psi(\boldsymbol{r},\boldsymbol{R};\boldsymbol{\rho})$ is a solution of the stationary Schrödinger equation:

$$H_{\rm sud}(\boldsymbol{r},\boldsymbol{R};\boldsymbol{\rho})\psi(\boldsymbol{r},\boldsymbol{R};\boldsymbol{\rho}) = (E-\varepsilon_{0j})\psi(\boldsymbol{r},\boldsymbol{R};\boldsymbol{\rho}) \tag{7}$$

with

$$H_{\rm sud}(\boldsymbol{r},\boldsymbol{R};\boldsymbol{\rho}) = T_R + H_{\rm el} - V_{\rm BeH}, \tag{8}$$

where we have neglected the terms $\nabla_\rho\psi$; this is the generalization to the vibrational motion of the energy sudden approximation, commonly employed for molecular rotation. In order to solve Eq. (7), one can introduce the centrifugal sudden approximation, which, together with the energy sudden one, yields the IOS approximation. In practice, working in the body-fixed frame (BFF), $\widetilde{X}\widetilde{Y}\widetilde{Z}$ with $\widehat{\widetilde{Z}} = \widehat{\boldsymbol{R}}$, and substituting the angular momentum operator L^2 by $L(L+1)$, we obtain

$$T_R \approx -\frac{1}{2\mu}\frac{1}{R}\frac{d^2}{dR^2}R + \frac{L(L+1)}{2\mu R^2}. \tag{9}$$

For the system H^++BeH, μ is the reduced mass,

$$\mu = \frac{m_{\rm H}+m_{\rm BeH}}{m_{\rm H}m_{\rm BeH}}, \tag{10}$$

and

$$\left[\frac{1}{R}\frac{d^2}{dR^2}R - \frac{L(L+1)}{R^2} - 2\mu(E-H_{\rm el}-\varepsilon_{0j})\right] \times \psi^L(\boldsymbol{r},R;\rho,\theta) = 0. \tag{11}$$

It must be noted that the solution of Eq. (11) depends parametrically on ρ and θ, and the second-order differential equation must be solved for a set of fixed values of these parameters. The sudden-vibration-IOS wave function ψ^L is now expanded in terms of a set of Born-Oppenheimer electronic wave functions:

$$\psi^L(\boldsymbol{r},R;\rho,\theta) = \sum_k F_k^L(R;\rho,\theta)\phi_k(\boldsymbol{r};R,\rho,\theta) \tag{12}$$

with

$$H_{\rm el}(\boldsymbol{r},R,\rho,\theta)\phi_j(\boldsymbol{r};R,\rho,\theta) = \epsilon_j(R,\rho,\theta)\phi_j(\boldsymbol{r};R,\rho,\theta). \tag{13}$$

Substitution of Eq. (12) into Eq. (11) leads to a set of second-order differential equations for the functions $F_k^L(R;\rho,\theta)$, from which one can calculate the corresponding scattering amplitudes $f_{if}(E,\hat{\boldsymbol{R}};\rho,\theta)$. It can be shown [42] that the degeneracy-averaged differential cross section for the $i0j \to fvj'$ transition is given by

$$Q_{i0j}^{fvj'}(E,\hat{\boldsymbol{R}}) = \frac{1}{2j+1}\frac{k_{fvj'}}{k_{i0j}}\sum_{m_j}|\langle vj'm_j|f_{if}|0jm_j\rangle|^2, \tag{14}$$

where $k_{fvj'}^2 = 2\mu(E-\epsilon_f-\varepsilon_{vj'})$ and the integrals are evaluated in the BFF and, since the scattering amplitudes f_{if} do not depend on the azimuthal angle of ρ, they vanish unless $m_j' = m_j$. Using closure [42,43], the cross section summed over all final rotational states has a very simple expression:

$$Q_{i0}^{fv}(E,\hat{\boldsymbol{R}}) = \sum_{j'}Q_{i0j}^{fvj'} = \frac{k_{fvj}}{k_{i0j}}\frac{1}{2}\int_{-1}^{1}d(\cos\theta)|\langle v|f_{if}|0\rangle|^2, \tag{15}$$

and the corresponding total cross section is expressed as

$$\overline{\sigma}_{i0}^{fv}(E) = \int d\hat{\boldsymbol{R}}\,Q_{i0}^{fv}(E,\hat{\boldsymbol{R}}) = \frac{1}{2}\int_{-1}^{1}d(\cos\theta)\sigma_{i0}^{fv}(E;\theta). \tag{16}$$

Assuming that the collision energy is large compared to the separations between the vibrational states, we can take

$$\frac{k_{fvj}}{k_{i0j}} \approx \frac{k_f}{k_i}, \tag{17}$$

which allows us to use the closure relation for the vibrational wave functions to obtain the differential and total cross sections for transitions to all vibrational states:

$$Q_f(E,\hat{\boldsymbol{R}}) = \sum_v Q_{i0}^{fv} = \frac{1}{2}\int_{-1}^{1}d(\cos\theta)\int d\rho|f_{if}|^2\chi_0^2, \tag{18}$$

$$\overline{\sigma}_f^{\rm Q}(E) = \frac{1}{2}\int_{-1}^{1}d(\cos\theta)\int d\rho\,\sigma_f^{\rm Q}(E,\rho,\theta)\chi_0^2. \tag{19}$$

In expansion (12), we have not taken into account the corrections due to the translation factors, which in the quantum-mechanical treatment are commonly introduced through a reaction coordinate formalism (see Ref. [44]). In particular, the substitution of the coordinate $\boldsymbol{R}$ by a common reaction coordinate $\boldsymbol{\xi}(\boldsymbol{R},\boldsymbol{r})$, in the appropriate way, ensures that the finite expansion (12) satisfies the correct boundary conditions.

B. Semiclassical treatment

Our semiclassical method has been applied in previous publications (see Ref. [45] and references therein). At impact energies $E \gtrsim 200$ eV/u, it is appropriate to employ the eikonal semiclassical approximation (e.g., Ref. [9]), where the projectile follows straight-line trajectories:

$$\boldsymbol{R} = \boldsymbol{b} + \boldsymbol{v}t \tag{20}$$

with impact parameter $\boldsymbol{b}$ and velocity $\boldsymbol{v}$. The relative velocity v is related with the collisional energy: $E = m_p v^2/2$, with m_p the projectile mass. In the eikonal treatment the electronic

motion is described by a wave function $\Psi^{\rm EIK}(\boldsymbol{r},\boldsymbol{\rho},t)$ solution of the equation

$$H_{\rm int}\Psi^{\rm EIK} - i\left.\frac{\partial\Psi^{\rm EIK}}{\partial t}\right|_{\boldsymbol{r},\boldsymbol{\rho}} = 0. \tag{21}$$

The sudden-vibrational (SV) approximation for the eikonal wave function was explained in detail in Ref. [20]. Within this approach, the eikonal wave function is expressed as

$$\Psi^{\rm SV}_{0jm} = \rho^{-1}Y_{jm}(\hat{\boldsymbol{\rho}})\chi_0(\rho)D(\boldsymbol{r},t)\sum_k a_k(t;b,E,\boldsymbol{\rho}) \times \phi_k(\boldsymbol{r};R,\rho,\theta)\exp\left[-i\int_0^t \epsilon_k dt'\right], \tag{22}$$

where $D(\boldsymbol{r},t)$ is a common translation factor (CTF) [46] that, in the present calculations, has the explicit form proposed in Ref. [47]. The collision wave function is expanded in terms of the molecular wave functions $\phi_j(\boldsymbol{r};R,\rho,\theta)$, eigenfunctions of $H_{\rm el}$ of Eq. (4). Substituting this expansion into Eq. (21), and neglecting the coupling terms proportional to $\nabla_\rho\phi_k$, leads, for each $\boldsymbol{\rho}$, to the system of differential equations

$$i\frac{da_j}{dt} = \sum_l [\boldsymbol{v}\cdot\boldsymbol{M}_{jl} + v^2 B_{jl}]a_l \exp\left[-i\int_0^t(\epsilon_l-\epsilon_j)dt'\right], \tag{23}$$

where $\boldsymbol{M}_{jl}$ are the nonadiabatic couplings, which include the correction terms due to the introduction of the CTF.

The system of differential equations (23) is solved for each $\boldsymbol{\rho}$ with the initial condition

$$\lim_{t\to-\infty} a_k(t;b,E,\boldsymbol{\rho}) = \delta_{ki}. \tag{24}$$

The transition probability to the final state $\Psi_{fvj'm'}$ is

$$\begin{aligned} P^{fvj'm'}_{i0jm}(b,E) &= \lim_{t\to\infty}\left|\left\langle\Psi_{fvj'm'}\middle|\Psi^{\rm SV}_{0jm}\right\rangle\right|^2 \\ &= \lim_{t\to\infty}\left|\int d\hat{\boldsymbol{\rho}}\, Y^*_{j'm'}(\hat{\boldsymbol{\rho}})Y_{jm}(\hat{\boldsymbol{\rho}}) \times\int d\rho\,\chi_v(\rho)\chi_0(\rho)a_f(t;b,E,\boldsymbol{\rho}) \times\exp\left[-i\int_0^t dt'(\epsilon_f-\mathcal{E}_f)\right]\right|^2, \end{aligned} \tag{25}$$

where $\mathcal{E}_f$ is the internal asymptotic excitation energy (nuclear plus electronic) of the system in the final state. The degeneracy-averaged transition probabilities are added over final rotational states to obtain the vibrationally resolved transition probabilities ($i\neq f$):

$$\begin{aligned} \overline{P}^{fv}_{i0}(b,E) &= \sum_{j'm'} P^{fvj'm'}_{i0jm} \\ &= \frac{1}{4\pi}\lim_{t\to\infty}\int d\hat{\boldsymbol{\rho}}\left|\int d\rho\,\chi_v(\rho)\chi_0(\rho)a_f(t;b,E,\boldsymbol{\rho}) \times\exp\left[-i\int_0^t dt'(\epsilon_f-\mathcal{E}_f)\right]\right|^2, \end{aligned} \tag{26}$$

where we have used the addition theorem for the spherical harmonics. Using closure for the vibrational functions, we can calculate the transition probability for populating all vibrational states:

$$\begin{aligned} \overline{P}_f(b,E) = \sum_v \overline{P}^{fv}_{i0} &= \frac{1}{4\pi}\lim_{t\to\infty}\int d\hat{\boldsymbol{\rho}}\int d\rho\,\chi_0^2(\rho) \times|a_f(t;b,E,\boldsymbol{\rho})|^2 \\ &= \frac{1}{4\pi}\int d\hat{\boldsymbol{\rho}}\int d\rho\,\chi_0^2(\rho)P_f(b,E;\boldsymbol{\rho}). \end{aligned} \tag{27}$$

We can define an orientation-dependent total cross section in the sudden approximation as an average over the values of the internuclear distance in the form

$$\sigma^{\rm SV}_f(E;\hat{\boldsymbol{\rho}}) = \int_0^\infty d\rho\,\sigma_f(E;\boldsymbol{\rho})\,\chi_0^2(\rho), \tag{28}$$

with

$$\sigma_f(E;\boldsymbol{\rho}) = 2\pi\int_0^\infty db\,b\,P_f(b,E;\boldsymbol{\rho}). \tag{29}$$

At high collision energies, the Franck-Condon (FC) approximation can be employed:

$$\sigma^{\rm FC}_f(E;\hat{\boldsymbol{\rho}}) = \sigma_f(E;\boldsymbol{\rho}_e), \tag{30}$$

where ρ_e is the equilibrium distance of the diatomic target molecule.

The orientation-averaged cross sections can be calculated by averaging $\sigma_f(E;\boldsymbol{\rho})$ or $\sigma^{\rm FC}_f(E;\hat{\boldsymbol{\rho}})$ [Eqs. (29) and (30)] over a set of nuclear trajectory orientations with a fixed-target orientation, as explained in Ref. [20]. An alternative, which is more simple from the computational point of view, is the semiclassical equivalent to the average procedure employed in the IOS-quantal treatment. To introduce this approximation, we assume that, for each trajectory and molecular orientation, the transition $i\to f$ takes place in a narrow interval of the projectile trajectory near the point of closest approach, characterized by a single value of the internal angle θ_0,

$$P_f(b,E;\boldsymbol{\rho}) \approx P^{\rm iso}_f(b,E;\rho,\theta_0), \tag{31}$$

and one can introduce the orientation-dependent cross section within this approximation as,

$$\sigma^{\rm iso}_f(E,\rho,\theta_0) = 2\pi\int_0^\infty db\,b\,P^{\rm iso}_f(b,E;\rho,\theta_0). \tag{32}$$

Since the couplings are independent of the azimuthal angle of $\boldsymbol{\rho}$ in the BFF, the orientation average in Eq. (28) can be carried out in the BFF as

$$\begin{aligned} \overline{\sigma}^{\rm SV}_f(E) \approx \overline{\sigma}^{\rm iso}_f(E) &= \frac{1}{2}\int_{-1}^1 d(\cos\theta)\sigma^{\rm iso}_f(E,\theta) \\ &= \frac{1}{2}\int_{-1}^1 d(\cos\theta)\int_0^\infty d\rho\,\sigma^{\rm iso}_f(E,\rho,\theta)\chi_0^2(\rho) \\ &= \pi\int_{-1}^1 d(\cos\theta)\int_0^\infty d\rho\,\chi_0^2(\rho) \times\int_0^\infty db\,b\,P^{\rm iso}_f(b,E,\rho,\theta), \end{aligned} \tag{33}$$

where we have simplified the notation by substituting θ_0 by θ. As in Eq. (11), the transition probabilities and cross sections depend parametrically on θ, and the collision is treated as a set of isotropic problems, similar to ion-atom collisions with the couplings evaluated for several values of θ, which is assumed to be constant along the collision. The FC approximation leads to

$$\overline{\sigma}_f^{\rm FC}(E) = \frac{1}{2}\int_{-1}^{1} d(\cos\theta)\sigma_f^{\rm iso}(E,\rho_e,\theta). \tag{34}$$

In practice, the transition probabilities $P_f^{\rm iso}$ of Eq. (32) are calculated by solving a system of differential equations similar to Eq. (23), where the energies (ϵ_j) and couplings ($\boldsymbol{M}_{jl}$, B_{jl}) only depend on the variable R, while θ and ρ are fixed parameters. This leads to a set of systems of differential equations that, for each value of ρ and θ, are formally identical to those found in ion-atom collisions:

$$\begin{aligned}\boldsymbol{v}\cdot\boldsymbol{M}_{jl}(R;\rho,\theta) = {}& \frac{v^2 t}{R}\langle\phi_j|\left.\frac{\partial}{\partial R}\right|_{\theta,\boldsymbol{\rho},\boldsymbol{r}}|\phi_l\rangle \\ & -\frac{bv}{R^2}\langle\phi_j|\left.\frac{\partial}{\partial\theta}\right|_{R,\boldsymbol{\rho},\boldsymbol{r}}|\phi_l\rangle \\ & +\text{CTF correction terms},\end{aligned} \tag{35}$$

with the derivatives calculated keeping $\boldsymbol{\rho},\boldsymbol{r}$ constant in the laboratory reference frame. Errea *et al.* [48] found that the angle-averaged cross section from Eq. (33) for EC in $H^+ + H_2$ collisions is in good agreement with the more sophisticated (and expensive) treatment of the anisotropy of the collisional system, where the average is performed over the relative orientations of $\hat{\boldsymbol{v}}$ and $\hat{\boldsymbol{\rho}}$, and taking into account explicitly the dependence of the couplings on $\hat{\boldsymbol{v}}\cdot\hat{\boldsymbol{\rho}}$ along the trajectory, but this point has not been checked yet for other systems. A similar approximation has been employed to treat ion collisions with large biomolecules (e.g., Refs. [49,50]), where the dynamical calculation is performed with energies and couplings evaluated at a fixed orientation of the molecule with respect to the projectile velocity vector.

It must be noted that, although Eqs. (19) and (33) are formally similar, the former one has been derived by using the centrifugal sudden approximation while the Coriolis couplings are not neglected in the semiclassical calculation [see Eq. (35)]. This difference precludes that quantal and semiclassical treatments lead in general to the same results. The validity of this approximation has been discussed in previous works for $H^+ + H_2$ collisions [35], where it was found that the cross sections obtained from quantal (IOS) and eikonal semiclassical calculations agree in the range of collision energies 200 eV $< E <$ 400 eV, and therefore both trajectory effects and centrifugal sudden approximation are not relevant. In general, it is expected that the semiclassical treatment, including rotational couplings, is more accurate at high energies than the IOS one.

III. MOLECULAR CALCULATIONS

A. Potential-energy curves of BeH

In order to check the accuracy of our molecular data for BeH_2^+, we have compared our results for BeH with those of Pitarch-Ruiz *et al.* [51], who carried out a full-configuration-interaction (CI) calculation with a large basis set combining atomic natural orbitals (ANOs) and Rydberg functions. Since we are studying collisions with BeH in its ground electronic state, only doublet states are relevant, and we compare the corresponding potential energy curves (PECs) with our results, obtained with the 6-31++G** basis set for Be taken from Ref. [52], the Basis Set Exchange website described in Ref. [53], and Roos Augmented Double Zeta ANO [54] for H, using the program MELD [39]. We perform, for both BeH and BeH_2^+ systems, full-CI calculations with the occupancy of the lowest Be $1s^2$ frozen. The energies obtained in both calculations differ by at most 0.01 hartree. In studying collisions, the relevant quantities are the differences between the energies of the electronic states. These differences are compared with those of Ref. [51] in Fig. 2. At each R, the small discrepancies between both calculations are quite similar for all states, which points to the effect of the frozen core approximation employed in our calculation.

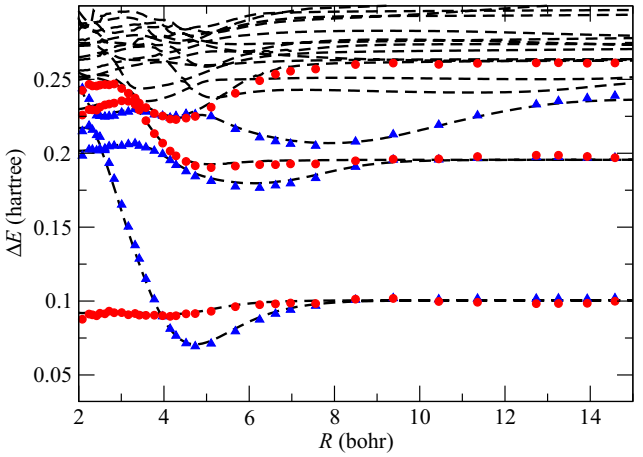

FIG. 2. Comparison between the energy differences $E_i - E_0$ of the BeH molecular states (symbols) of Ref. [51] with those obtained in the present calculation (dashed lines). Bullets correspond to $^2\Sigma$ states and triangles to $^2\Pi$ states.

B. Asymptotic electronic structure of the triatomic system BeH_2^+

A qualitative description of the mechanism of the EC reaction can be deduced from the energies of the triatomic system in the asymptotic limit as the distance R (see Fig. 1) between the projectile and the BeH center of mass goes to infinity. The corresponding energy curves are the PECs of the BeH (doublets) system together with the PECs of the ion BeH^+ (singlets and triplets systems), to which we add 0.5 hartree corresponding to the energy of H(1s). Figure 3 presents these curves, where the energy of the state BeH($^2\Sigma^+$), which is the entrance channel of reaction (1), is the thick dashed line. The equilibrium bond length for the BeH ($^2\Sigma^+$) molecule is around $\rho_e = 2.568$ bohrs. We can see in Fig. 3 that there are three EC channels close in energy to the entrance channel that support bound states and with equilibrium distances near ρ_e. There is also a repulsive charge-transfer channel whose energy crosses that of the entrance channel at $R \approx 6$ bohrs. We have

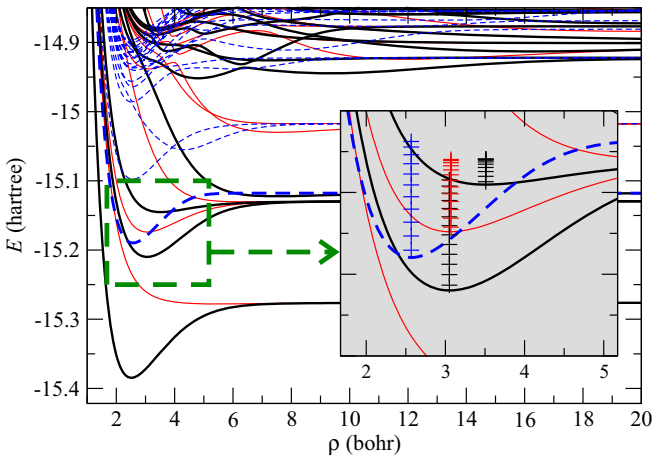

FIG. 3. PECs of the H^++BeH system in the limit as the distance between H^+ and BeH goes to infinity. The solid lines are the energies of the states dissociating into H+BeH^+ with the BeH^+ in singlets (thick black lines) and triplets (thin red lines). The dashed lines are the energies of the doublet states of BeH. The inset is a zoom of the squared area delimited with a long-dashed line and also includes ("+" symbols) the energies of the vibrational levels of the four electronic states.

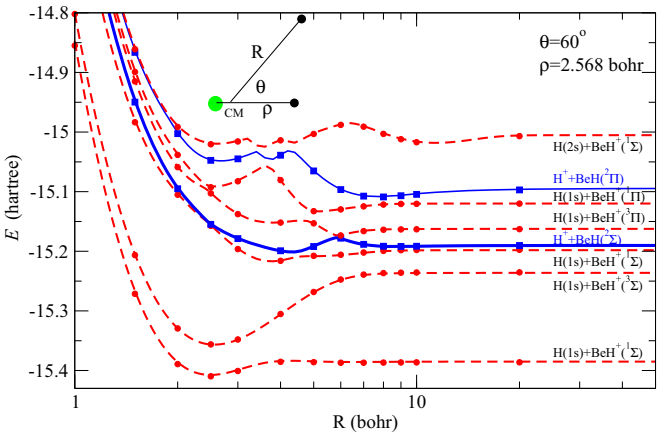

FIG. 4. Cuts of the PESs of the doublet states of $(HBeH)^+$ along the line with $\rho = 2.568$ bohrs and $\theta = 60^\circ$ as functions of R. The solid lines are the energies of the states that correlate to H^++BeH and the dashed lines those of the EC channels that correlate to H+BeH^+. Lines, frozen-core full-CI calculation; solid symbols, multireference single- and double-excitation CI calculation.

calculated the vibrational levels of the bound electronic states using Le Roy's LEVEL program [55] (assuming $J = 0$) and the results are included in the inset of the figure. At low collision energies, the EC reaction will take place through transitions from the ground vibrational level to quasiresonant vibrational levels of BeH^+, namely,

$$H^+ + BeH(X\,^2\Sigma^+, v = 0) \rightarrow H + BeH^+(2\,^1\Sigma^+, v' = 3,4), \tag{36}$$

$$H^+ + BeH(X\,^2\Sigma^+, v = 2) \rightarrow H + BeH^+(2\,^3\Sigma^+, v'' = 0). \tag{37}$$

These mechanisms are similar to those found in $H^+ + H_2$ collisions at low energies (see Ref. [35] and references therein), where we found that the EC total cross section shows a local maximum at $E \approx 45$ eV that is a consequence of transitions between vibronic levels. Accordingly, we expect that the transitions (36) will furnish the low-E mechanism with an increase of the cross section with respect to that obtained from extrapolation of the SV results.

In Fig. 3, we also observe the presence of a crossing between the PECs of channels $H^+ + BeH(X\,^2\Sigma^+)$ and $H + BeH^+(2\,^1\Sigma^+)$ at ρ slightly lower than ρ_e. This crossing in the qualitative illustration corresponds to an asymptotic conical intersection between the potential energy surfaces of the triatomic system. It must be noted that the conical intersection is accessible within the vibrational ground-state wave function. The presence of an asymptotic conical intersection was previously found in the H_3^+ system (see Ref. [56]). Figure 3 shows another asymptotic conical intersection between the PESs of the entrance channel and that dissociating into $H + BeH^+(2\,^3\Sigma^+)$ at a BeH internuclear distance, $\rho \approx 3.2$ bohrs, which is not accessible from the vibrational ground state of the electronic entrance channel.

C. The triatomic system for $\theta = 60°$ and $\rho = \rho_e$

The perfect agreement between full-CI energies of the three-center system calculated with MELDF and the multireference single- and double-excitation CI calculation using the MRDCI code is illustrated in Fig. 4 for $\theta = 60^\circ$ and $\rho = \rho_e$. These PECs allow us to discuss the mechanism of the EC reaction for the particular trajectory with the proton approaching the nuclear center of mass of the target molecule with a specific angle $\theta = 60^\circ$ with respect to the BeH bond direction (see Fig. 1). We have chosen this particular orientation because it was found in Ref. [48] that the cross section $\sigma_f^{\rm iso}(E,\rho,\theta = 60^\circ)$ is close to the orientation average $\overline{\sigma}_f^{\rm iso}(E,\rho)$. The energy of the entrance channel that dissociates into $H^+ + BeH(1\sigma^2 2\sigma^2 3\sigma^1; X\,^2\Sigma^+)$ is the lowest solid line that corresponds to the fourth state (ϕ_4). At large R, the energy of ϕ_4 is very close to that of ϕ_3, which correlates to the charge-transfer channel $H + BeH^+(1\sigma^2 2\sigma^1 3\sigma^1; 2\,^1\Sigma^+)$, and presumably it should have a Demkov-type interaction around $R \simeq 10$ bohrs, where the PECs start to diverge. The relative positions of the energies of these two states vary when changing ρ. In particular, the energy of the entrance channel is asymptotically lower than that of the charge transfer channel for $\rho < \rho_c$, where ρ_c is the Be-H distance of the conical intersection shown in Fig. 3. At lower R, the energy of the entrance channel approaches that of the state dissociating into $H + BeH^+(1\,^3\Sigma^+)$, which furnishes an alternative mechanism of the EC process.

From the energy diagram of Fig. 4, and similar ones for other orientations and Be-H distances, it is clear that the main exit channels are the states $2\,^1\Sigma^+$ and $1\,^3\Sigma^+$. The most important configuration of these states is $1\sigma^2 2\sigma^1 3\sigma^1$, which means the electron is captured from the orbital 2σ. Capture

from the highest occupied molecular orbital, 3σ, leads to the formation of $BeH^+(1\,^1\Sigma^+)$ and is expected to be less relevant.

D. Dynamical couplings

In our calculations, the CTF included in expansion (22) is a symmetric function with respect to the permutation of the electronic coordinates $\boldsymbol{r}_i$ of the form

$$D(\boldsymbol{r},t) = \exp[\mathrm{i}U(\boldsymbol{r},t)] \tag{38}$$

with

$$U(\boldsymbol{r},t) = \sum_i (f\boldsymbol{v}\cdot\boldsymbol{r}_i - 1/2 f^2 v^2 t) \tag{39}$$

and the switching function

$$f(\boldsymbol{r}_i,R) = g(R)\boldsymbol{r}_i\cdot\hat{\boldsymbol{R}}, \tag{40}$$

where

$$g(R) = \frac{R}{R^2+\beta^2}, \tag{41}$$

and $\beta = 2.0$ bohrs in the present work. As explained in Eq. (35), the nonadiabatic couplings are calculated for fixed values of ρ and θ. Including the CTF corrections, the radial component is given by

$$\mathcal{R}_{jl} = \langle\phi_j|\frac{\partial}{\partial\widetilde{Z}}\Big|_{\widetilde{X},\rho,\theta,\boldsymbol{r}}|\phi_l\rangle - \frac{1}{2}[2g - Rg^2](\epsilon_l-\epsilon_j)\langle\phi_j|\sum_i z_i^2|\phi_l\rangle, \tag{42}$$

and the rotational one by

$$\mathcal{S}_{jl} = \langle\phi_j|\frac{\partial}{\partial\widetilde{X}}\Big|_{\widetilde{Z},\rho,\theta,\boldsymbol{r}}|\phi_l\rangle - g(\epsilon_l-\epsilon_j)\langle\phi_j|\sum_i x_i z_i|\phi_l\rangle, \tag{43}$$

where it is assumed that the electronic wave functions are exact eigenfunctions of $H_{\rm el}$ and

$$\frac{\partial}{\partial\widetilde{X}} = \frac{1}{R}\frac{\partial}{\partial\theta}. \tag{44}$$

The particular CTF of Eqs. (38) and (40) yields also correction terms proportional to v^2, see Eq. (23), that come from the matrix elements of ∇U and $\partial U/\partial t$, and are proportional to electronic quadrupole matrix elements.

On the other hand, since the switching function (40) is also used to define the common reaction coordinate in the quantal treatment, the radial and rotational couplings are identical in semiclassical and quantal formalisms. The derivative couplings in Eqs. (42) and (43) have been evaluated numerically [40] for $R \geqslant 0.5$ bohr, where the molecular states are clearly identified. In any case, very small distances are only reached in collisions with small impact parameter (low-L partial waves in the quantal formalism) that does not significantly contribute to the total cross section. An explicit check of the numerical differentiation procedure is shown in Fig. 5, where we compare the couplings $\mathcal{R}_{jl}$, evaluated with the techniques implemented in MELDF and MRDCI codes and with the same Gaussian basis set.

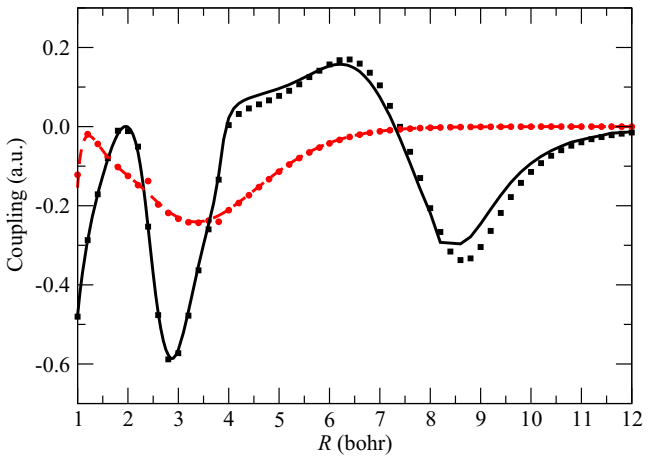

FIG. 5. Nonadiabatic couplings between the adiabatic states ϕ_3 and ϕ_4 (solid line) and ϕ_5 and ϕ_6 (dashed line) for $\rho = 2.568$ bohrs and $\theta = 180^\circ$, obtained with the full-CI calculation, as functions of R, compared to multireference single- and double-excitation CI calculation (solid symbols).

As an illustration, we show in Fig. 6(a) the nonadiabatic couplings between the third and the fourth adiabatic states, which are, respectively, the main exit channel and the entrance channel (Fig. 4) of the EC process. For $\rho = 2.568$ bohrs and $\theta = 60^\circ$, the radial coupling shows a small maximum at $R \approx 8$ bohrs that is due to the Demkov-type interaction (e.g., Ref. [57]) between both states. There is a maximum in both components at $R \approx 4.5$ bohrs, which is a consequence of the avoided crossing between the corresponding PECs. The most conspicuous structures arise at $R \approx 2.45$ bohrs; the radial coupling exhibits a high peak, while the rotational one shows a double-peak structure, which are characteristics of a conical intersection between the corresponding PESs. In this particular case, the conical intersection seam appears for isosceles-triangle geometries (C_{2v} symmetry). There is another peak

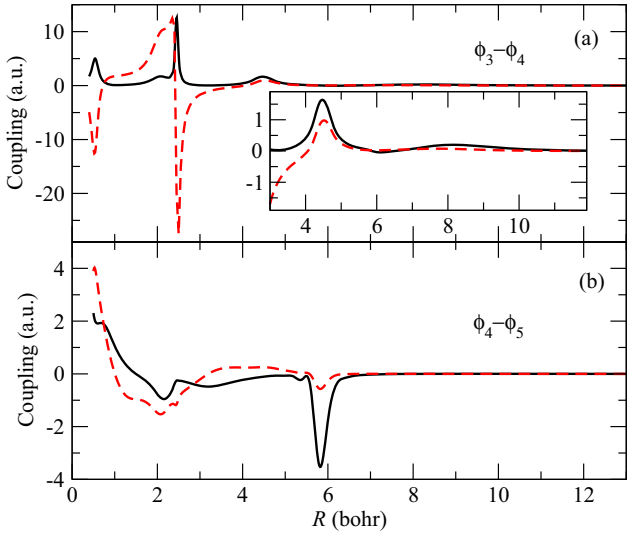

FIG. 6. Nonadiabatic radial (solid lines) and rotational (dashed lines) couplings between the adiabatic states (a) ϕ_3 and ϕ_4 and (b) ϕ_4 and ϕ_5 for $\rho = 2.568$ bohrs and $\theta = 60^\circ$ as functions of R.

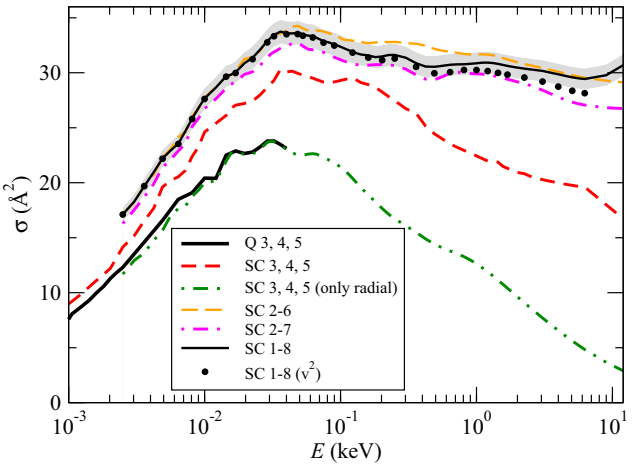

FIG. 7. Orientation-averaged total EC cross section as a function of the impact energy, calculated at the FC level and different basis sets, as indicated in the figure. SC denotes semiclassical calculations and Q quantal calculations. The lines correspond to calculations including only couplings proportional to v-CTF. The bullets are the results obtained including also the CTF corrections proportional to v^2. Shaded area is ±3% of solid line.

at $R \approx 0.55$ bohr, which comes from an additional avoided crossing not shown in Fig. 4. The couplings between states ϕ_4 and ϕ_5 are plotted in Fig. 6(b). One can note peaks in both components at $R \approx 5.80$ bohrs in the pseudocrossing; there is also an avoided crossing at $R < 0.5$ bohr that explains the increase of the couplings at the lowest distances of our calculation. The remaining structures are due to the changes in the character of the adiabatic states in regions where nonadiabatic couplings with other states are important, for instance, near the ϕ_3-ϕ_4 conical intersection.

IV. DYNAMICAL CALCULATIONS

A. Franck-Condon orientation-averaged cross sections

At high impact energies it is appropriate to employ the FC approximation, where the orientation-dependent total cross sections are $\sigma_f^{\rm iso}(E,\rho_e,\theta)$ and they are orientation averaged using Eq. (34). Moreover, the FC calculations are useful to gauge the validity of some approximations mentioned in Sec. II and to check the convergence of the expansion.

Figure 7 presents the total EC cross sections at the FC level:

$$\overline{\sigma}^{\rm FC}(E) = \sum_f \overline{\sigma}_f^{\rm FC}(E). \tag{45}$$

The figure shows the results obtained with different basis sets: the three-state basis $\{\phi_3 - \phi_5\}$ is a minimal basis that includes the entrance channel (ϕ_4) and the two main exit channels (ϕ_3 and ϕ_5), see also Fig. 4; the five-state basis $\{\phi_2 - \phi_6\}$ adds two EC channels; the six-state basis includes one excitation channel (ϕ_7); and the eight-state basis has two additional EC channels. In all these calculations we have neglected the coupling terms proportional to v^2 [B_{jl} in Eq. (23)]. The results including these terms are only plotted for the eight-state calculation. We can note that both calculations agree within a ±3% error for $E \leqslant 5$ keV, as indicated by the shaded area.

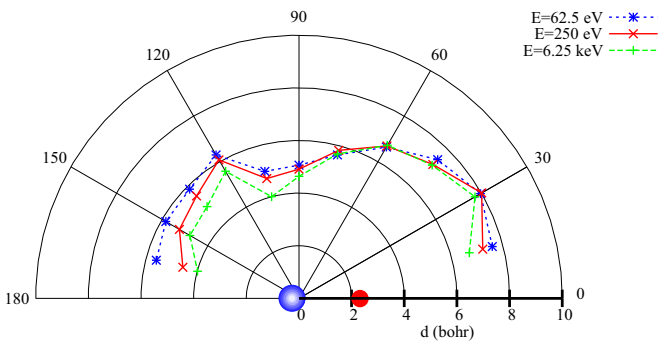

FIG. 8. Polar plot of d [Eq. (47)] as a function of θ for the three collision energies indicated in the figure. The spheres indicate the positions of the target nuclei.

Accordingly, the collision mechanism can be discussed by considering only the couplings M_{jl}, shown in Sec. III. One can also notice the good agreement between five-, six- and eight-state calculations for $E \leqslant 10$ keV, which confirms the convergence of our calculation. At $E > 10$ keV, the eight-state cross section shows a sudden increase that suggests that the population of the high-lying states, in particular that of ϕ_8, could correspond to ionization, not correctly described by the L^2-integrable basis.

We include in Fig. 7 some results of $\overline{\sigma}^{\rm Q}(E)$:

$$\overline{\sigma}^{\rm Q}(E) = \sum_f \overline{\sigma}_f^{\rm Q}(E) = \frac{1}{2}\sum_f \int_{-1}^{1} d(\cos\theta)\sigma_f(E,\rho_e,\theta), \tag{46}$$

obtained with the quantal formalism [see Eqs. (6), (12), and (19)] and the three-state basis. Although the comparison with the three-state semiclassical result is unsatisfactory, it merges with this semiclassical calculation when the Coriolis couplings are removed. This comparison clearly indicates that the semiclassical eikonal approximation is valid and the differences with the quantal results are due to the centrifugal sudden approximation employed in the latter approach. The slow merging of the results with and without rotational couplings in Fig. 7 also indicates the importance of rotational couplings at $E > 2.5$ eV.

B. Franck-Condon orientation-dependent EC total cross section

The dependence of the EC total cross section on the angle θ is illustrated in Fig. 8, where we plot the values of the radius, d, related with the cross section:

$$d = \sqrt{\frac{1}{\pi}\sum_f \sigma_f^{\rm iso}(E,\rho_e,\theta)}. \tag{47}$$

As it has already been explained in Sec. II, the results for specific values of θ are obtained from energies and couplings calculated along lines with constant θ, which can be viewed as ion trajectories approaching the target center of mass along lines with fixed θ in Fig. 8. In practice, the calculation is carried out for each value θ by integrating the system of coupled differential equations (23) for each impact parameter with the corresponding coupling matrix elements $M_{jl}(R,\rho_e,\theta)$. For

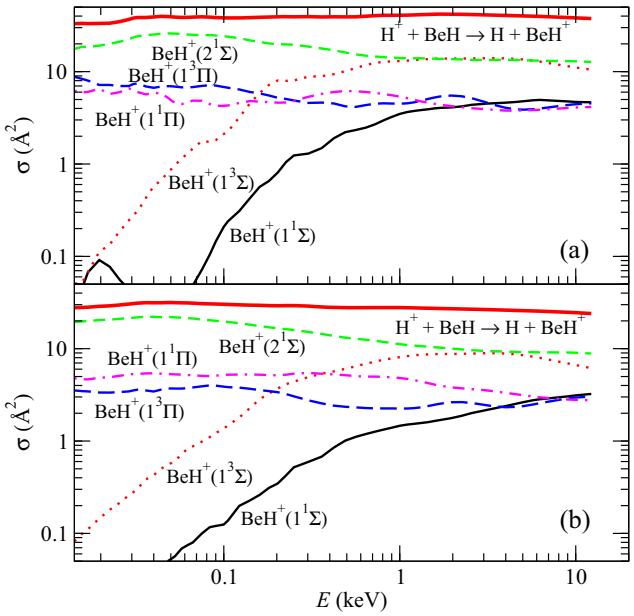

FIG. 9. State-selected EC cross sections in Å^2 as functions of the impact energy. (a) FC calculation with $\theta = 60^\circ$, $\sigma_f^{\rm iso}(E,\rho_e,\theta = 60^\circ)$. (b) Orientation-averaged FC calculation, $\overline{\sigma}_f^{\rm FC}$.

all collision energies, the calculations with $\theta \approx 90^\circ$ yield the lowest EC cross sections because the dynamical calculation is carried out with the couplings evaluated in a direction perpendicular to the internuclear axis where the electronic density is relatively small. The largest cross sections are found for trajectories with small θ when the data (energies and couplings) correspond to a projectile approaching the molecule near the H nucleus. This behavior is a consequence of the dominant mechanism discussed in Sec. III C, where the electron is captured from the molecular orbital 2σ that has the largest electronic density near the H nucleus. An intermediate situation is found for large values of θ, where the electron is predominantly captured from the density located near the Be nucleus.

C. State-selected EC cross sections

We present in Fig. 9 the EC partial cross sections $\sigma_f^{\rm iso}(E,\rho_e,\theta = 60^\circ)$, obtained in a FC semiclassical calculation with the eight-state basis set and $\theta = 60^\circ$. At low energies, the dominant exit channel is BeH$^+$($2\,^1\Sigma^+$), in agreement with the fact that very efficient transitions take place from the state ϕ_4 (the entrance channel) to the state ϕ_3 that correlates to BeH$^+$($2\,^1\Sigma^+$)+H($1s$) (see Fig. 4). As E increases, the cross section for populating BeH$^+$($1\,^3\Sigma^+$)+H($1s$) also increases as a consequence of the fact that $\phi_3 \to \phi_2$ transitions become more efficient. In fact, the cross sections for transitions to BeH$^+$($2\,^1\Sigma^+$)+H($1s$) and BeH$^+$($1\,^3\Sigma^+$)+H($1s$) are very similar at $E > 1$ keV. Besides, the states $1\,^{1,3}\Pi$ are formed in transitions $\phi_4 \to \phi_5 \to \phi_6$. From the asymptotic structures of these channels the population of states $1\,^{1,3}\Pi$ involves a two-electron transition: one electron is captured from the 2σ molecular orbital and another electron is excited from 3σ to 1π, which explains that the corresponding cross sections

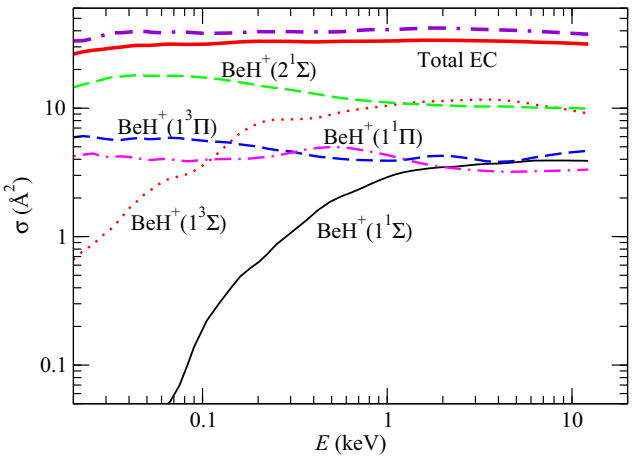

FIG. 10. State-selected EC cross sections $\sigma_f^{\rm iso}(E,\theta = 60^\circ)$, evaluated using the vibrational sudden approach of Eqs. (33) and (48). The thick dash-dotted line is the FC result for the total EC cross section.

are small compared to those for populating BeH$^+$($2\,^1\Sigma^+$, $1\,^3\Sigma$). However, although the EC into BeH$^+$($1\,^1\Sigma^+$) involves a one-electron transition, in which the electron is captured from the singly occupied 3σ molecular orbital, the energy gap between the PECs of states ϕ_1 and ϕ_4 precludes the direct transition; it takes place through the sequence $\phi_4 \to \phi_2 \to \phi_1$. It explains the small cross section and the fact that in Fig. 9 the lines for the cross sections for populating BeH$^+$($1\,^3\Sigma^+$) and BeH$^+$($1\,^1\Sigma^+$) are almost parallel.

D. Sudden vibrational calculations

We plot in Fig. 10 the EC orientation-dependent partial cross sections, $\sigma_f^{\rm iso}$, calculated using the SV approach; they are obtained by substituting Eq. (32) into Eq. (28):

$$\sigma_f^{\rm iso}(E,\theta = 60^\circ) = \int_0^\infty d\rho\, \sigma_f^{\rm iso}(E,\rho,\theta = 60^\circ)\chi_0^2(\rho). \quad (48)$$

The FC results of Fig. 9(a) qualitatively agree with the SV ones of Fig. 10. However, there are clear differences for some partial cross sections at low E. For instance, the SV cross section for populating BeH$^+$($1\,^3\Sigma^+$) is larger than that from the FC calculation by almost an order of magnitude for $E <$ 0.1 keV. This difference comes from the ρ dependence of the PECs, as can be noticed from the asymptotic energies plotted in Fig. 3, the increase of the energy of the state BeH$^+$($1\,^3\Sigma$) as ρ decreases approaching that of the entrance channel at $\rho < \rho_e$, which accordingly leads to higher transition probabilities and to larger contributions of the small ρ values to the integral over ρ in Eq. (48). On the contrary, the cross sections for populating BeH$^+$($1\,^{1,3}\Pi$) states in Fig. 10 are smaller than the corresponding ones in Fig. 9(a) for $E < 0.1$ keV, as a consequence of the increase of the energies of these two states (see Fig. 3) as ρ decreases, which lowers the transitions from the entrance channel. We also compare in Fig. 10 the total EC cross sections calculated at the FC level,

$$\sigma^{\rm iso}(E,\rho_e,\theta = 60^\circ) = \sum_f \sigma_f^{\rm iso}(E,\rho_e,\theta = 60^\circ), \quad (49)$$

and the corresponding SV one:

$$\sigma^{\rm iso}(E,\theta = 60^\circ) = \sum_f \sigma_f^{\rm iso}(E,\theta = 60^\circ). \qquad (50)$$

At low energies, the EC process is dominated by transitions to the three-center electronic state dissociating into $BeH(2\,^1\Sigma)$, well represented by the FC approximation, which leads to an almost constant error of about 20% of the FC total EC cross section with respect to the more accurate SV result.

V. SUMMARY AND CONCLUSIONS

In this work we have calculated total and state-resolved integral cross sections for electron capture in H^++BeH collisions by employing an eight-state molecular basis. The calculations have been carried out in the framework of the sudden approximation for rotation and vibration and with rectilinear nuclear trajectories. We have performed exploratory quantal (IOS) calculations that indicate that the semiclassical approximation is appropriate for $E > 25$ eV, but the accuracy of the IOS treatment is limited by the approximation of neglecting the Coriolis couplings. Although this approximation is not relevant at $E < 1$ eV, at these low energies, transitions between quasiresonant vibronic levels will probably furnish the main mechanism of the EC process, and prevent the extrapolation to low energies of the present SV calculation. The vibronic transitions will increase the cross section, and the cross section plotted in Fig. 7 for $E < 25$ eV is a lower bound of the total cross section. Therefore, the EC cross section is sizable and may be relevant to plasma modeling. The usefulness of the FC approximation has been gauged by comparing SV and FC orientation-dependent cross sections [Figs. 10 and 9(a), respectively]. Although we have found general good agreement for the total cross section and the cross section for EC into the main exit channel, the validity of the FC approximation is in general limited to impact energies above 1 keV for the partial cross sections.

The main exit channel of the electron-capture reaction is the formation of $H(1s)+ BeH^+(2\,^1\Sigma^+)$, which involves the electron transfer from the 2σ molecular orbital to the orbital $H(1s)$, which is almost degenerate; this molecular orbital has the largest electronic density located near the H nucleus. It can be noted that the total cross section is large (≈ 25 Å^2) compared with that of $H^+ + H_2$ [35], which has a maximum of $\sigma \approx 10$ Å^2 at $E \approx 5$ keV and decreases very quickly with $\sigma < 1$ Å^2 at $E = 100$ eV. The cross section is also one order of magnitude larger than the one calculated for $H^+ + Be$ in Ref. [58]. The value is, however, close to the cross section obtained for $H^+ + H(1s) \approx 25$ Å^2 at $E = 100$ eV [59], in accordance with the dominant $H(1s)$ character of the 2σ orbital. On the other hand, at low energies, the partial cross section for populating $BeH^+(1\,^3\Sigma^+)$ is small because of the large energy difference with the entrance channel, but, as E increases, the contribution of this channel to the EC total cross section becomes significant. For $E > 1$ keV the populations of states $BeH^+(1\,^3\Sigma^+)$ and $BeH^+(2\,^1\Sigma^+)$ are similar, and since the state $1\,^3\Sigma^+$ is dissociative [60], it means that about 50% of the electron-transfer collisions lead to the molecular fragmentation into $Be^+(2s)$ and $H(1s)$.

Previous theoretical studies have focused on collisions with H_2 molecules, where the isotropic approximation [Eqs. (33) and (34)] allows one to simplify the average over molecular orientations, but this approach has not been checked for heteronuclear targets. One can note that in collisions with homonuclear molecules, and assuming the six-trajectory approximation of Ref. [20], where θ is a function of t, the energies and couplings are symmetric or antisymmetric upon time inversion; if we assume that the transitions take place in a narrow region of ion-molecule separations at $t \approx \pm t_0$, they correspond to a single value of $\theta(t_0)$. However, the present calculation for collisions with BeH shows a significant dependence of the EC cross sections $\sigma_f^{\rm iso}(E,\rho_e,\theta)$ on the angle θ (see Fig. 8). In particular, the comparison of our EC cross sections for θ and $\pi - \theta$ indicates that a calculation following a given trajectory may not be well simplified by considering transitions for a representative value θ_0, as assumed in Eq. (31). Although this condition is probably too restrictive, the dependence of the EC cross sections on θ casts some doubts on the validity of the isotropic approximation, and a detailed calculation with the couplings varying along the trajectory is required.

ACKNOWLEDGMENTS

This work has been partially supported by a Project Universidad Autónoma de Madrid—Banco Santander de Cooperación Interuniversitaria con Asia and Ministerio de Economía y Competitividad (Spain) (Grant No. ENE2014-52432-R). We also acknowledge the computational hosting service of the Centro de Computación Científica de la Universidad Autónoma de Madrid.

[1] ITER Organization, http://www.iter.org
[2] G. Matthews, J. Nucl. Mater. **438**, S2 (2013).
[3] S. Brezinsek, J. Nucl. Mater. **463**, 11 (2015).
[4] C. Björkas, K. Vörtler, K. Nordlund, D. Nishijima, and R. Doerner, New J. Phys. **11**, 123017 (2009).
[5] C. Björkas, D. Borodin, A. Kirschner, R. K. Janev, D. Nishijima, R. Doerner, and K. Nordlund, Plasma Phys. Controlled Fusion **55**, 074004 (2013).
[6] S. Brezinsek, M. Stamp, D. Nishijima, D. Borodin, S. Devaux, K. Krieger, S. Marsen, M. O'Mullane, C. Bjoerkas, A. Kirschner, and JET EFDA contributors, Nucl. Fusion **54**, 103001 (2014).
[7] S. Brezinsek, A. Widdowson, M. Mayer, V. Philipps, P. Baron-Wiechec, J. Coenen, K. Heinola, A. Huber, J. Likonen, P. Petersson, M. Rubel, M. Stamp, D. Borodin, J. Coad, A. Carrasco, A. Kirschner, S. Krat, K. Krieger, B. Lipschultz, C. Linsmeier, G. Matthews, K. Schmid, and JET contributors, Nucl. Fusion **55**, 063021 (2015).
[8] D. Borodin, S. Brezinsek, I. Borodkina, J. Romazanov, D. Matveev, A. Kirschner, A. Lasa, K. Nordlund, C. Björkas, M.

Airila, J. Miettunen, M. Groth, and M. Firdaouss, Nucl. Mater. Energy **9**, 604 (2016).
[9] B. H. Bransden and M. H. C. McDowell, *Charge Exchange and the Theory of Ion-Atom Collisions* (Clarendon Press, Oxford, UK, 1992).
[10] T. Minami, T.-G. Lee, M. S. Pindzola, and D. R. Schultz, J. Phys. B **41**, 135201 (2008).
[11] A. Jorge, J. Suárez, C. Illescas, L. F. Errea, and L. Méndez, Phys. Rev. A **94**, 032707 (2016).
[12] J. Loreau, S. Ryabchenko, and N. Vaeck, J. Phys. B **47**, 135204 (2014).
[13] V. Sidis, Adv. At. Mol. Opt. Phys. **26**, 161 (1989).
[14] D. J. Kouri, in *Atom-Molecule Collision Theory: A Guide for the Experimentalist*, edited by R. B. Bernstein (Springer, Boston, 1979), pp. 301–358.
[15] A. Dickinson, Comput. Phys. Commun. **17**, 51 (1979).
[16] M. Baer, G. Niedner-Schatteburg, and J. P. Toennies, J. Chem. Phys. **91**, 4169 (1989).
[17] P. S. Krstić, Phys. Rev. A **66**, 042717 (2002).
[18] L. F. Errea, L. Fernández, L. Méndez, B. Pons, I. Rabadán, and A. Riera, Phys. Rev. A **75**, 032703 (2007).
[19] R. Schinke, Chem. Phys. **24**, 379 (1977).
[20] L. F. Errea, J. D. Gorfinkiel, A. Macías, L. Méndez, and A. Riera, J. Phys. B **30**, 3855 (1997).
[21] M. Kimura, Phys. Rev. A **32**, 802 (1985).
[22] R. Shingal and C. D. Lin, J. Phys. B **22**, L659 (1989).
[23] T. Kusakabe, L. Pichl, R. J. Buenker, M. Kimura, and H. Tawara, Phys. Rev. A **70**, 052710 (2004).
[24] L. Meng, C. O. Reinhold, and R. E. Olson, Phys. Rev. A **42**, 5286 (1990).
[25] C. Illescas and A. Riera, Phys. Rev. A **60**, 4546 (1999).
[26] Y. D. Wang, J. H. McGuire, and R. D. Rivarola, Phys. Rev. A **40**, 3673 (1989).
[27] H. T. Schmidt, D. Fischer, Z. Berenyi, C. L. Cocke, M. Gudmundsson, N. Haag, H. A. B. Johansson, A. Källberg, S. B. Levin, P. Reinhed, U. Sassenberg, R. Schuch, A. Simonsson, K. Støchkel, and H. Cederquist, Phys. Rev. Lett. **101**, 083201 (2008).
[28] J. S. Alexander, A. C. Laforge, A. Hasan, Z. S. Machavariani, M. F. Ciappina, R. D. Rivarola, D. H. Madison, and M. Schulz, Phys. Rev. A **78**, 060701 (2008).
[29] K. N. Egodapitiya, S. Sharma, A. Hasan, A. C. Laforge, D. H. Madison, R. Moshammer, and M. Schulz, Phys. Rev. Lett. **106**, 153202 (2011).
[30] A. Hasan, S. Sharma, T. P. Arthanayaka, B. R. Lamichhane, J. Remolina, S. Akula, D. H. Madison, and M. Schulz, J. Phys. B **47**, 215201 (2014).
[31] A. Hasan, T. Arthanayaka, B. R. Lamichhane, S. Sharma, S. Gurung, J. Remolina, S. Akula, D. H. Madison, M. F. Ciappina, R. D. Rivarola, and M. Schulz, J. Phys. B **49**, 04LT01 (2016).
[32] A. Igarashi and L. Gulyás, J. Phys. B **50**, 035201 (2017).
[33] L. F. Errea, A. Macías, L. Méndez, I. Rabadán, and A. Riera, Phys. Rev. A **65**, 010701 (2001).
[34] G. Niedner, M. Noll, J. P. Toennies, and C. Schlier, J. Chem. Phys. **87**, 2685 (1987).
[35] X. Urbain, N. de Ruette, V. M. Andrianarijaona, M. F. Martin, L. F. Menchero, L. F. Errea, L. Méndez, I. Rabadán, and B. Pons, Phys. Rev. Lett. **111**, 203201 (2013).
[36] N. Sisourat, I. Pilskog, and A. Dubois, Phys. Rev. A **84**, 052722 (2011).
[37] C. Illescas, L. F. Errea, L. Méndez, B. Pons, I. Rabadán, and A. Riera, Phys. Rev. A **83**, 052704 (2011).
[38] M. Murakami, T. Kirchner, M. Horbatsch, and H. J. Lüdde, Phys. Rev. A **85**, 052704 (2012).
[39] E. R. Davidson, in *MOTECC, Modern Techniques in Computational Chemistry*, edited by E. Clementi (ESCOM Publishers B. V., Leiden, 1990).
[40] J. F. Castillo, L. F. Errea, A. Macías, L. Méndez, and A. Riera, J. Chem. Phys. **103**, 2113 (1995).
[41] R. J. Buenker and R. A. Phillips, J. Mol. Struct. THEOCHEM **123**, 291 (1985).
[42] G. A. Parker and R. T. Pack, J. Chem. Phys. **68**, 1585 (1978).
[43] J. M. Bowman, J. Chem. Phys. **66**, 296 (1977).
[44] J. B. Delos, Rev. Mod. Phys. **53**, 287 (1981).
[45] E. Rozsályi, L. F. Errea, L. Méndez, and I. Rabadán, Phys. Rev. A **85**, 042701 (2012).
[46] S. B. Schneiderman and A. Russek, Phys. Rev. **181**, 311 (1969).
[47] L. F. Errea, L. Mendez, and A. Riera, J. Phys. B **15**, 101 (1982).
[48] L. F. Errea, A. Macías, L. Mendez, I. Rabadan, and A. Riera, Int. J. Mol. Sci. **3**, 142 (2002).
[49] M. C. Bacchus-Montabonel, M. Łabuda, Y. S. Tergiman, and J. E. Sienkiewicz, Phys. Rev. A **72**, 052706 (2005).
[50] M.-C. Bacchus-Montabonel, J. Phys. Chem. A **117**, 14169 (2013).
[51] J. Pitarch-Ruiz, J. Sánchez-Marin, A. M. Velasco, and I. Martin, J. Chem. Phys. **129**, 054310 (2008).
[52] Environmental Molecular Science Laboratory, https://bse.pnl.gov/bse/portal
[53] K. L. Schuchardt, B. T. Didier, T. Elsethagen, L. Sun, V. Gurumoorthi, J. Chase, J. Li, and T. L. Windus, J. Chem. Inf. Model. **47**, 1045 (2007).
[54] P.-O. Widmark, P.-Å. Malmqvist, and B. O. Roos, Theor. Chim. Acta **77**, 291 (1990).
[55] R. J. L. Roy, J. Quantum Spectrosc. Radiat. Transfer **186**, 167 (2017).
[56] M. Baer, in *Advances in Chemical Physics* (John Wiley & Sons, New York, 2007), pp. 187–241.
[57] E. E. Nikitin and S. Y. Umanskii, *Theory of Slow Atomic Collisions* (Springer-Verlag, Berlin, 1984).
[58] P. Barragán, L. F. Errea, L. Méndez, I. Rabadán, and A. Riera, J. Phys. B **41**, 225202 (2008).
[59] J. H. Newman, J. D. Cogan, D. L. Ziegler, D. E. Nitz, R. D. Rundel, K. A. Smith, and R. F. Stebbings, Phys. Rev. A **25**, 2976 (1982).
[60] C. H. Liu, J. G. Wang, and R. K. Janev, J. Phys. B **43**, 144006 (2010).